The Caspian Sea Journal
ISSN: 1578-7899

Volume 10, Issue 1, Supplement 4 (2016) 145-153

Comparing the Performance and Lifetime of Co/GNS and Co/CNT Catalysts in Fischer-Tropsch Synthesis

Fatemeh Hasanpour,
School of chemistry, College of Science, University of Tehran, Tehran, Iran
Corresponding Author: fatemehasanpour@ut.ac.ir)
Somayeh Taghavi,
School of chemistry, University of Semnan, Semnan, Iran,
Ahmad Tavasoli
School of chemistry, College of Science, University of Tehran, Tehran, Iran,

ABSTRACT─ Graphene nanosheets (GNS) and carbon nanotubes (CNTs) were used as cobalt Fischer-Tropsch synthesis (FTS) catalyst support. 20 wt. % cobalt was loaded on GNS and CNTs by wet impregnation method. The physico-chemical properties of supports and the catalysts were investigated by different methods including ICP, BET, XRD, TPR and H2 chemisorption. The activity, selectivity and stability of the catalysts were evaluated in a fixed bed micro-reactor at 18 bars. The measurements were carried out at 220°C and H2/CO ratio of 2. Prior to the reaction, the catalysts reduced at 400°C for 16h in H2 flow. The results showed that, in comparison with Co/CNTs catalyst, using GNS as cobalt FTS support increased the CO conversion, increased the C5+ selectivity and improved the catalyst stability with the same loading of Co. XRD results showed that the average clusters size decreased from 10.8 to about 9.4 nm when GNS were used as catalyst. Also, GNS as the support shifted the reduction temperature of cobalt oxide species to lower temperatures. FT synthesis rate increased by about 15%; the product distribution shifted to the higher molecular weight hydrocarbons, compared to CNTs supported catalyst. 720 h continuous FT synthesis decreased 22% of the initial activity of the graphene-supported cobalt catalyst. However, the same duration, decreased the CO conversion for CNTs supported catalyst by 34%.

KEYWORDS: Fischer–Tropsch synthesis, Cobalt, GNS, CNTs, Activity, Stability

Introduction

Fischer-Tropsch synthesis (FTS) is the catalytic hydrogenation of carbon monoxide which has attracted intermittent attention as a source of low-sulfur fuel [1]. 'CH' monomer, produced by hydrogenation of CO, creates a variety of hydrocarbons including a wide range of chain lengths and functional groups [2]. The active metals used in FTS are Fe, Co, and Ru. Ru results very active catalysts but its high price and limited world resources reject it's industrial application [3]. Iron is available and its price makes it a suitable candidate for industrial purposes but its activity in water-gas shift reaction causes a high deactivation rate [4-5]. Cobalt is an expensive metal in comparison with iron but the higher activity and stability make it a good choice for FTS [6-7]. In addition to catalytic activity and products selectivity, catalyst deactivation is an important parameter for industrial catalyst development. The activity of cobalt-based FTS catalysts changes during their operation because of sintering; re-oxidation of cobalt, surface oxidation; formation of stable compounds between cobalt and the support, e.g., cobalt aluminate; surface reconstruction; formation of carbon species on the cobalt surface; carbiding; and poisoning [8]. Different materials have been used as catalyst support but during the last 10 years. Recently, the use of carbon nano-materials as supports in catalysis has been increased. This is mainly due to their unique structure and intrinsic properties, including high specific surface areas, chemical and electrochemical inertness and easy surface modification. Recently, Graphene Nano Sheet (GNS) has shown unique properties and remarkable tunability in supporting a variety of metallic and bimetallic nanoparticle catalysts in heterogeneous catalysis [9-10]. In this study the 20wt.%Co/GNS catalyst prepared by the incipient impregnation method. The physico-chemical characteristics, performance and stability of the catalyst were evaluated, and the results were compared with the results of Co/CNTs catalyst.

Experimental

Catalyst preparation

Multiwall CNTs and Graphene Nano Sheets (GNS) were used as support for preparation of the catalysts. Prior to catalyst preparation, the supports were treated with 30% HNO_3 refluxed at 120°C overnight, washed with distilled water several times, and dried at 120°C for 6 h. The aqueous solution of cobalt ($Co(NO_3)_2 \cdot 6H_2O$ 99.0% Merck) was dispersed on GNS and CNTS to obtain catalysts (20 wt. % cobalt) by impregnation method (Imp). Then, catalysts were dried at 120°C for 2h and calcined at 400°C (in argon) for 4h with a heating rate of $10^{o}C \cdot min^{-1}$.

Catalyst characterization

The FTIR absorption technique for confirming the formation of functional groups was conducted on a Bruker ISS-88. A smooth transparent pellet of 0.5–5% of CNTs or GNS mixed with 95–99.5% potassium bromide (KBr), was made and the infrared beam passed through this pellet. The metal loadings of the calcined catalysts were performed using Varian VISTA-MPX inductively coupled plasma-optical emission spectrometry (ICP-OES) instrument. For this purpose, 0.02 g of sample was dispersed in 5 ml of nitric acid (Merck 65%) and 5 ml hydrochloric acid (Chem-Lab, 37%). The temperature of the mixture was kept at 40–50°C for 2 h. The resulting mixture was filtered and washed several times with distilled water. The filtrate solution was diluted with dionized water up to 250 ml (acid digestion). The cobalt loadings of the calcined catalysts were measured by an Inductively Coupled Plasma Atomic Emission Spectroscopy (ICP-AES) system. Average crystallite size of the calcined powders was determined by XRD. BET surface area and pore volume were determined by N_2 physisorption using a Micro-meritics ASAP 2010 automated system. 0.1 g catalyst sample was degassed in the system at 100ºC for 1 h and then at 300ºC for 2 h prior to analysis. The phases and particle sizes of the crystals present in the catalysts were analyzed by X-ray diffraction (XRD) experiments using a Philips analytical X-ray diffractometer (XPert MPD) with monochromatized Cu/Kα radiation, 2θ angles from 20° to 80°. The Debye-Scherrer formula was applied to Co_3O_4 peaks at 2θ = 36.8, in order to calculate the average particle sizes.The H2-TPR profiles of the catalysts were performed in order to study the reducibility of the metal species in the catalysts. The calcined catalyst sample (0.05 g) was first purged in a flow of Helium at 140°C to remove traces of water and gases exist in catalyst, and then cooled to 40°C. Then, the temperature-programmed reduction (TPR) of each sample was performed using 5% H_2 in Ar stream at a flow rate of 40 ml/min at atmospheric pressure using Micrometrics TPD-TPR 2900 analyzer equipped with a thermal conductivity detector (TCD), heating at a linearly programmed rate of 10°C/min up to 850°C. The amount of chemisorbed hydrogen was measured using the Micromeritics TPD-TPR 290 system. 0.22 g of the calcined fresh and calcined used catalysts were reduced at 400°C for 12 h and then cooled to 100°C under hydrogen flow. Then the flow of hydrogen was switched to argon at the same temperature, which lasted about 30 min in order to remove the weakly adsorbed hydrogen. Afterwards the temperature programmed desorption (TPD) of the samples was obtained by increasing the temperature of the samples, with a ramp rate of 10 8C/min, to 400°C under the argon flow. The TPD spectrum was used to determine the cobalt dispersion and its surface average crystallite size. After the TPD of hydrogen, the sample was re-oxidized at 400°C by pulses of 10% oxygen in helium to determine the extent of reduction. It is assumed that Co^o is oxidized to Co_3O_4. The calculations are summarized below. The calculated dispersion and diameter are corrected by the percentage reduction [11-13].

$$\text{Dispersion (\%)} = \frac{Number\ of\ CO0\ atoms\ on\ the\ surface \times 100}{number\ of\ CO0\ atom\ in\ sample}$$

$$\text{Fraction reduced} = \frac{O2\ uptake\left(\frac{mole}{gr}cat\right) \times \frac{2}{3} \times atomic\ weight}{Percentage\ metal}$$

$$\text{Diameter (nm)} = \frac{6000}{Density \times maximum\ area \times dispersion}$$

Reaction testing

The FTS reactions were carried out in a fixed-bed stainless steel reactor (Fig.1). The reactor temperature was controlled via a PID temperature controller. Brooks 5850 mass flow controllers were used to add H_2 and CO at desired flow rates into the reactor. Pressure was controlled by a backpressure valve in the outlet stream. The catalyst (0.5 g) was loaded to the reactor. Catalysts activation was conducted in a flow of H_2 at 400ºC in atmospheric pressure. Catalysts were tested in 18 bar, 220ºC under 60 mL/min flow of reactants (H_2/CO=2). The gaseous products were analyzed by an online gas chromatography (Varian CP 3800). Liquid products, collected in a cold and hot trap, were removed every 24h and analyzed by a GC equipped with a FID detector and a capillary column. After 720 h , the first FT reaction step, the flow of synthesis gas was switched to hydrogen and catalyst was re-reduced at the same condition similar to the first reduction step (second treatment step). The second FT synthesis step was carried out and the activity and selectivity of the system were measured. After that, the flow of synthesis gas was switched off and the catalytic bed was washed by helium flow for 3 h at 270 ºC to remove the heavy waxes inside the catalyst pores. The reactor was cooled to 20 ºC and the catalyst was passivated with pulses of dry air [14]. The used catalyst was discharged and characterized.

Results and discussion

Characterization of fresh and used catalysts

Results of FTIR are given in Fig. 2. This figure shows the infrared spectrum of the purified GNS. The peak at 1600 cm^{-1} due to the stretching mode of double-bonds (C=C) in the GNS backbone. Peaks at 2921 cm^{-1} (both C-H anti symmetric and symmetric stretch for CH3 and CH2), 664 cm^{-1} (C-H) are shown [15]. There is a peak at 664 cm^{-1} bands of C-H bending mode. The main reason for this peak is the defects which are formed when the GNS is significantly functionalized.

The infrared spectrum of the purified and CNT has been shown in Fig. 2. As shown, there are some basic similarity in spectrums that regarded to CNT backbone including peaks at 1601 cm^{-1}, 2850-2950 cm^{-1} and 597cm^{-1} related to (C–H)(alkanes), (C-H) respectively. [15,16]. The results of ICP, BET and pore size distribution for the supports, the fresh calcined and used catalysts are shown in Table 1. According to ICP analyses, the metal contents of the calcined fresh and used catalysts were close to the nominal Co metal content of 20.0 wt. % and the metal loss for catalysts during FTS is insignificant. Table 1 shows the results of the BET surface areas, pore volumes, pore sizes of fresh catalysts. As shown, the BET surface area of GNS is more than that of the CNTs (495vs. 260 m^2/g). Due to high surface area of GNS the average cobalt crystallite size in Co/GNS catalyst is significantly lower and this situation might inhibit the cobalt crystallites agglomeration. Smaller particle and consequently the higher dispersion will provide more cobalt available atoms for FTS reaction in the Co/GNS catalyst in comparison with the Co/CNTs catalyst [17,18]. Results of surface area measurements for the used catalysts are given in the Table 1. These results show that the BET surface areas of the Co/GNS and Co/CNT catalysts was decreased from 298 to 264 m^2/g and 197 to 153 m^2/g. XRD patterns of the fresh Co/GNS and Co/CNTs nano catalysts are shown in Fig.3. For the calcined fresh Co/GNS and Co/CNT nano catalysts, the peaks at 2θ of 25.0º and 43.0º correspond to graphite layers, while the other peaks in the pattern of fresh Co/GNS are related to different crystal planes of Co_3O_4 [19-21]. The peak at 36.8º is the most intense peak of Co_3O_4 No peak corresponding to the formation of cobalt-support compounds in the XRD pattern of the fresh Co/GNS nano catalyst was observed. Also, XRD patterns of the used Co/GNS and Co/CNT nano catalysts are shown in Fig. 3. As shown, the resulting patterns for the used catalysts are very complex. In the XRD pattern of the used Co/GNS nad Co/CNT nano catalysts, support peaks appeared at 2θ values of 25.0º and 43.0º. The peaks at 2θ values of 51.1º and 75.8º correspond to the metallic cobalt (Coº) [19,22]. Also, the peak at 2θ value of 46.9º correlates well with Co_2C. The presence of Co_2C can be attributed to a Co-carbon reaction during the carbon monoxide dissociative adsorption. The peaks at 2θ values of 36.8º and 42.5º correspond to Co_3O_4 and CoO [23]. Although a fraction of cobalt clusters may be oxidized in presence of significant amount of water formed during FT synthesis with high conversions, some amount of the cobalt oxide in the used sample probably is formed during the discharge and passivation step at room temperature. The intensities of the peaks for tow catalysts are different. Table 1 show that 720 h continuous FT synthesis increased the average crystal sizes for both catalysts. However, the crystal growth was more significant in the case of Co/CNT catalyst. Temperature programmed reduction (TPR) determines the reducibility of the catalysts in H_2 atmosphere. TPR profiles of the fresh calcined catalysts, used catalysts and the reduction peak temperatures are shown in Fig.4. It can be observed that the reduction process of the catalysts occurs in two distinct stages. The first peak is attributed to the reduction of Co_3O_4 to CoO, and the second peaks related to the reduction of CoO to Coº and the reduction of cobalt species that interact with the support. In the TPR profile of fresh Co/CNTs catalyst, the first peak centered at 350 °C, whereas the second broader peak centered at 510°C [24]. This figure shows that, using GNS as cobalt catalyst support will shift both TPR peaks to the lower temperatures at 260 and 450°C, showing an easier reduction process. The unpaired electrons on GNS surface, which are ready to be shared with other electrons, makes reduction of cobalt oxides easier and shifts the reduction peak temperatures to lower temperatures [25]. Table 2 shows the quantitative results of H_2 consumption for catalysts in H_2-TPR. The hydrogen uptake increases significantly using GNS as cobalt catalyst support. In agreement with the results of TPR, results indicate that a remarkable improvement in the percentage reduction is obtained by switching to GNS support with the same Co loading. While the dispersion of the cobalt crystallites calculated based on the total amount of cobalt increases significantly, the average cobalt particle size decreases, which is due to the lower degree of agglomeration of the cobalt crystallites in Co/GNS supported catalyst [26]. These results are in agreement with the results of XRD patterns. Higher dispersion and lower cobalt cluster size will increase the number of sites available for FT reaction in the Co/GNS catalysts in comparison with the Co/CNT with the same cobalt loading. In TPR patters the area under the second reduction peak (through integration) is three times of the area of the first reduction peak. Therefore, we concluded that cobalt crystalline phase is mostly Co_3O_4 [27]. The TPR pattern for the used catalyst shows that the reduction peaks of used catalysts shifted to lower temperatures after 720 h of FT synthesis. The first TPR temperature peak decreased from 350 to 320°C and the second TPR peak decreased from 510 to 450°C for Co/CNTs catalyst and for Co/GNS catalyst TPR temperature peak decreased sequentially from 260 to 240°C and from 450 to 400°C. A low reduction temperature can be due to either an easier reduction of larger cobalt particles (XRD) or to the presence of less stable oxides (XRD). Therefore, it has been shown that the interaction of the metal oxide nanoparticles with the inner and outer CNTs surfaces can affect the reduction behavior of the metal oxides [28]. The electron deficiency of the interior CNT surface can facilitate the reduction of the metal oxides located in the inner surface of the tubes as compared with the particles located in the outer surface of the tubes. Sintering of the particles attached to the outer surface of the tubes during FT synthesis increased the ratio of the number of particles located inside the tubes to the number of particles located on the outer surface, be another reason for the lower TPR peak temperature of the used calcined catalyst [24, 28]. Also, the results of H_2 chemisorption and oxygen titration tests for the catalysts are shown in Table 2. Comparing the results for both fresh catalysts, clearly reveal that the hydrogen uptake increases by using GNS as the support. In agreement with the TPR outcome, the results in this table indicate that a remarkable improvement in the degree of reduction is obtained by switching to GNS support with the same cobalt loading. While the dispersion of the cobalt crystallites, calculated based on the total amount of cobalt and the amount of reduced cobalt, increases significantly, the average cobalt particle size decreases, which is due to higher surface area of graphene and lower degree of

agglomeration of the cobalt crystallites. Also Using GNS as cobalt catalyst support resulted an increase in the number of active sites of the metal. The increase in the number of active sites for the catalyst followed the same trend as the dispersion and increase the amount of hydrogen adsorbed. Results show that the hydrogen consumption for the used catalysts is lower than that of their corresponding fresh calcined catalysts. Both the reduction in percentage and dispersion calculated based on the total cobalt decreased significantly. Continues FT synthesis for 720 h decreased the dispersion of Co/GNS nano catalyst form 22.3 to 19.8 % and that of Co/CNTs nano catalyst from 20.1 to 15.9 %. According to results in Table 2 which are in agreement with the data obtained from XRD patterns, the average diameter of cobalt nano particles increased especially in the case of Co/CNTs nano catalyst and the rate of sintering or cluster growth for the Co/CNT nano catalyst is higher than that for the Co/GNS nano catalyst.

Activity and product selectivity results

The %CO conversion and products selectivity for Co/GNS and Co/CNTs catalysts are given in Table 3 and Fig.5. It should be noted that catalytic activity and product selectivity were calculated within the first 24 h of the reactor run. The CO conversion depends mainly on cobalt precursor, pretreatment conditions and the type of support [18]. Table 3 reveals that cobalt catalyst supported on GNS significantly enhances the CO conversion and FT synthesis rate. CO conversion and the FTS rate on Co/GNS catalyst show an increase of about 12 and 25% as compared to the Co/CNTs catalyst, which are in accordance with the hydrogen uptake, percentage reduction and percentage dispersion reported in Table 2. The catalytic activity, FTS rate and CO conversion are strongly dependent on the number of surface reduced active cobalt sites [29]. The higher surface area of GNS support cause better dispersion of cobalt, smaller Co particles and more active sites and higher activity according to H_2-chemisorbtion, XRD, TPR results [30]. Distribution of FTS products on Co/GNS and Co/CNTs catalysts is presented in Fig.5. As is shown, the selectivity of light hydrocarbons is reduced by using GNS as the support. Product distribution shows a slight shift to higher molecular weight hydrocarbons in Co/GNS catalyst. Co/GNS catalyst improves the C_{5+} selectivity 6% and CH_4 and light gas selectivity of the Co/GNS catalyst decreased 23% and 12% comparing with Co/CNTs catalyst [31]. In the case of GNS supported catalyst, increasing CO conversion increases H_2O concentration, and it can decrease the surface H/CO ratio. Decomposition of H_2O creates O and OH species on the surface. These intermediates and CO molecules are adsorbed strongly which consequently, reduce the adsorption of H, which in turn leads to the chain growth and production of heavier hydrocarbons [32]. On the other hand, different supports according to their structures have different internal mass transfer limitations. Briefly the unique grapheme structure (nano sheets) and the fact that there is no limitation of internal mass transfer can facilitate the mass transfer during the reaction and considered to be the main reason for the excellent results [33].

Stability

Fig. 6 presents the CO conversion changes with the duration of FT synthesis for Co/GNS and Co/CNT nano catalysts. As it can be seen, for both catalysts the %CO conversion sharply decreases in the first days, and then levels off. The deactivation curve sloped steeply at first and then moderately and finally very slowly. This Figure shows that, for the Co/GNS catalyst a plateau region is reached after 6 days which indicates that the loss of active sites decreases significantly during the first 144 h of continues FT synthesis. However, for the Co/CNTs catalyst, the area of little variation region is reached after about 5 days. The loss of activity for the first deactivation step can be simulated with following linear correlation.

Co/GNS catalyst: $X_{CO}= -0.4711\ T_{(day)}+ 76.23$

Co/CNT catalyst: $X_{CO}= -4.588\ T_{(day)}+ 68.01$

For both catalysts, the linear deactivation mode suggests that the deactivation rate is zero order. It implies that the deactivation is unrelated to the number of the catalyst active sites and caused by exterior factors. For the FT synthesis catalysts, the loss of active sites during the first deactivation step is caused by water-induced oxidation of cobalt. Also, this deactivation process entails cobalt redox transformations and the formation of more refractory forms of oxidized cobalt generated by cobalt-support interactions [23,34]. The extent of this type of deactivation depends on the partial pressure of water produced during FT synthesis. Although the TPR and XRD results showed that the Co/CNT catalyst is more susceptible to re-oxidation and cobalt-support interactions, the Equations 4 and 5 and the results in Fig.6 show that the rate of deactivation in the first deactivation step is higher for the Co/CNT catalyst. Larger deactivation observed for the Co/CNT catalyst can be attributed to the higher partial pressure of water as an exterior factor produced during FT synthesis and present in the catalytic bed of the reactor [35-37]. In addition, higher conversions in the case of Co/GNS catalyst can increase the partial pressure of water that must result in higher catalyst deactivation rates. This behavior may be explained by the highly hydrophobic nature of GNS [38,39]. The hydrophobic GNS surface can reduce water deposition on the catalyst surface and prevent reoxidation of Co to a large extent.

When time-on-stream exceeded 144 h and 120 h for Co/CNT, the catalyst deactivation could be simulated with a power law expression:

Co/GNS: $X_{CO}= 75.224\ T_{day}^{-0.025}$

Co/CNT: $X_{CO}= 54.487\ T_{day}^{-0.054}$

Assuming the deactivation rate is:

$dX/dt = K X^n$

After integration and data reduction by least square fit, the power order (n) can be determined as (41) and (19.5) for the Co/GNS and Co/CNT catalysts, respectively, for the second deactivation step. These values are in the range that ordinary metal catalysts would experience during sintering [40]. Also, the results of H_2 chemisorptions and re-oxidation tests showed in Table 2 confirm the cluster growth during 720 h reaction. FT synthesis temperature is low to boost the cluster growth at the catalyst surface but it seems that water vapor increases the oxidation reduction cycles on the catalyst surface which in turn leads to cluster growth or sintering.However, the lower power order of 19.5 for the Co/CNTs catalyst demonstrates the higher rate of sintering in comparison to that for the Co/GNS catalyst. Hydrophobic surface of Co/GNS causes lower P_{H2O} on the surface and makes it difficult to form larger agglomerates. Fig.7 shows the methane selectivity variations with reaction time. This figure displays that CH_4 selectivity slightly decreases with time on stream during 720 h FT synthesis at 220°C and 18 bars. Also, the contents in hot and cold traps were removed every 24 h and the hydrocarbon and water fractions separated and analyzed. Fig.7. shows the variations of liquid C_5^+ selectivity with time on stream during FT synthesis. This figure shows that the C_5^+ selectivity slightly increases during 720 h FT synthesis. It has been shown [40] that the larger cobalt particles producing during FT synthesis are more selective to higher molecular weight hydrocarbons and smaller cobalt particles are selective to methane and light gaseous hydrocarbons. Higher rate of sintering of the cobalt particles in the case of Co/CNT catalyst is believed to be the main reason for greater enhancement of C_5^+ selectivity and suppression of CH4. In order to determine the contribution of each deactivation aspect on the overall deactivation of the catalyst, the used catalysts were again regenerated at 400°C. Subsequently, the reactor was cooled to 220°C and the second FT synthesis step was carried out under similar conditions as the previous synthesis step and CO conversions and FTS rate were measured. Table 3 presents CO conversions and FTS rates for both catalysts after regeneration and 24 h FT synthesis. The results show that the regeneration of the used Co/GNS catalyst at 400°C increased CO conversion from 72.67% to 74.52%. In the case of Co/CNTs catalyst regeneration at 400°C increased CO conversion from 45.4% to 64.12%. Thus, for Co/GNS about 2.2% of activity loss and for the Co/CNT about 5.7% of activity loss is not recoverable which may be attributed to the sintering of cobalt particles. Therefore, it is conceivable that the extent of irreversible deactivation in Co/CNTs is larger than that of the Co/GNS catalyst.

Conclusion

The results of this research reveal that the FT synthesis productivity of the Co/GNS catalyst is significantly greater than that of the Co/CNTs catalyst. TPR results showed that, deposition of cobalt nano particles on the GNS, shifts the reduction steps to lower temperatures and the reducibility of the catalysts improved significantly. According to H2 chemisorption, the catalyst prepared on GNS had a narrow particle size distribution and consequently larger dispersion in comparison with the CNTs Supported cobalt catalyst. Improvements on the uniformity of the catalyst particles in the case of the catalyst prepared on functionalized GNS, leads to a higher CO conversion. However, the results of the used catalysts characterization, especially XRD and H_2 chemisorptions tests, showed that the rate of sintering or cluster growth is much higher for the Co/CNTs catalyst than that for the Co/GNS catalyst and the Co/CNTs catalyst is more susceptible for deactivation.

Table 1: ICP, BET, and Porosity and XRD data for the Fresh and Used Catalysts

Catalyst	BET Surface area (m^2/g)	Pore Volume (cm^3/g)	Pore size (nm)	Crystallite size(XRD) (nm)	Co percent (ICP)
GNS	495.9	1.462	12.22	_	_
Fresh Co/GNS	298.9	0.745	7.21	9.4	19.91
Used Co/GNS	264.2	0.421	6.91	10.9	19.87
CNTs	260.5	0.681	4.72	_	_
Fresh Co/CNT	197.3	0.428	4.16	10.8	19.94
Used Co/CNT	153.7	0.321	4.03	13.6	19.91

Table 2. H_2 adsorbed, %Reduction, %Dispersion and crystallite sizes of cobalt particles determined by H_2 TPD and pulse reoxidation of fresh calcined and used catalysts.

Catalyst	Mole H_2 Desorption/Gcat.	Mole O_2 Consumption/Gcat.	% Red.	%Dispersion	Dp/Nm (Red. Co)
Fresh Co/Cnt	223	1431	64.3	20.2	7.4
Used Co/Cnt	175	1183	56.9	15.9	9.1
Fresh Co/Gns	317	1742	73.6	22.3	5.7
Used Co/Gns	286	1594	66.9	19.8	6.9

Table 3. FT synthesis rate (gCH/ (gcat·h)) and CO conversion (%) after 24 and 720 h FT synthesis and after regeneration at 400ºC over the Co/GNS and Co/CNT nano catalysts (T =220ºC, P = 1.8MPa, H_2/CO = 2)

Catalyst	% CO conversion after 24 h	O/P	% CO conversion after 720 h	% CO conversion after 720 h and regeneration at 400ºC (%)	FT synthesis rate (g CH/ (g cat.h)) after 24 h	FT synthesis rate (g CH/ (g cat.h)) after 720 h	FT synthesis rate (g CH/(g cat.h)) after 720 h and regeneration at 400ºC (%)
Co/GNS	76.23	0.93	72.67	74.52	0.356	0.328	0.345
Co/CNT	68.01	0.87	45.4	64.12	0.285	0.198	0.268

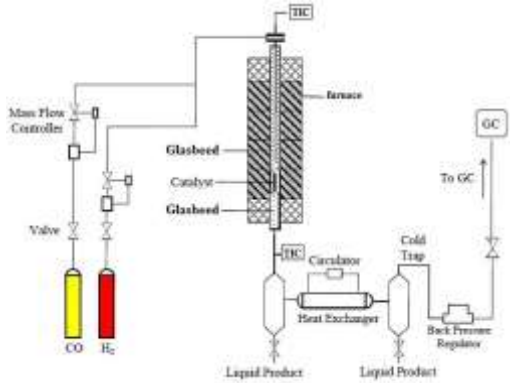

Fig.1. Catalyst test system

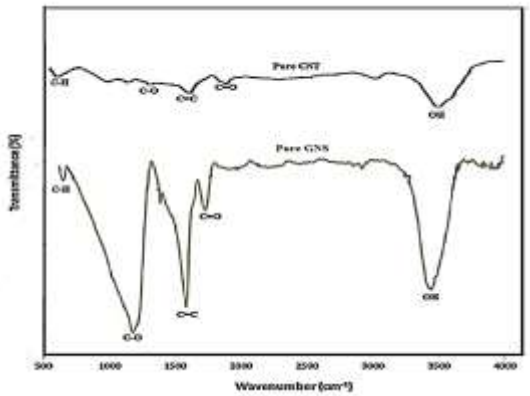

Fig. 2. FTIR spectrum of Pure GNS and pure CNT

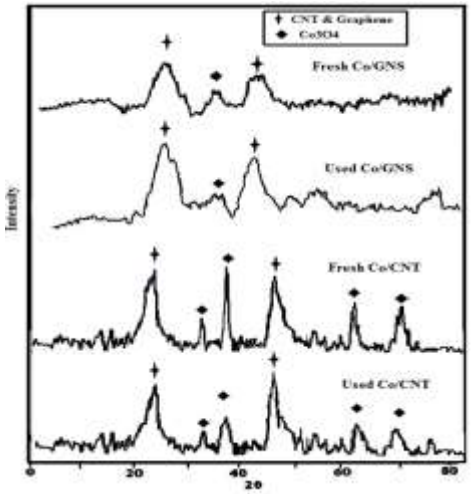

Figure 3. XRD patterns of the fresh and used Co/GNS and Co/CNT catalysts

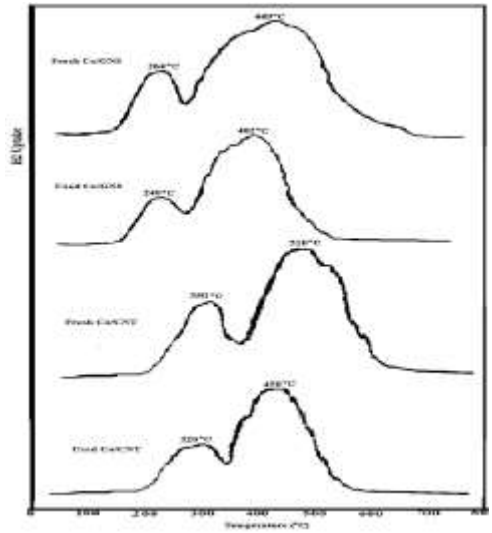

Figure 4. TPR patterns of different catalysts from 30 to 900 oC.

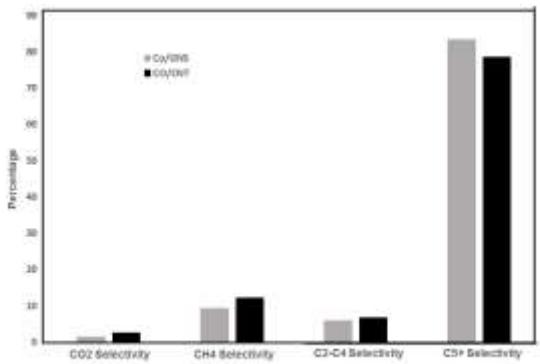

Figure 5. Product selectivity for Co/GNS and Co/CNT catalysts for first 24 h (T = 220 ºC, P =1.8MPa, H2/CO = 2).

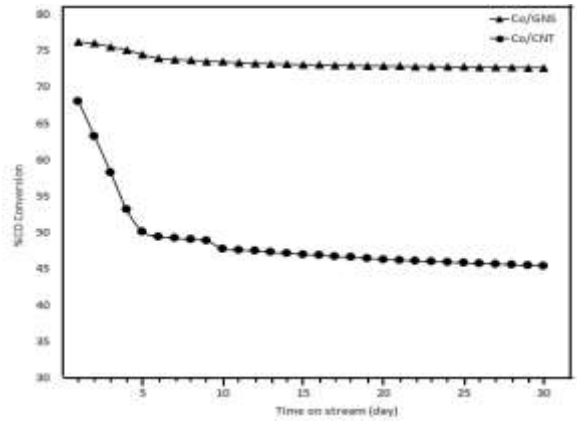

Figure 6. CO conversion against time-on-stream for Co/GNS and Co/CNT catalysts (T = 220ºC, P = 1.8MPa, H2/CO = 2)

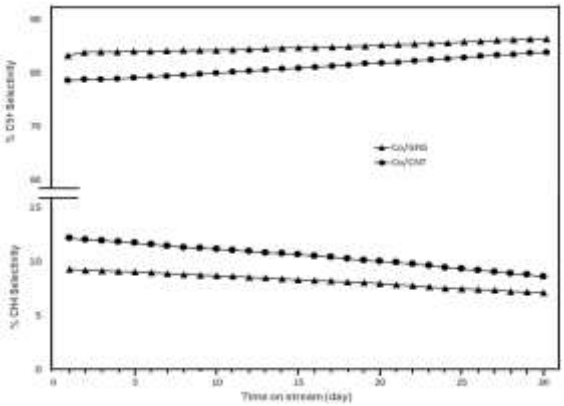

Figure 7. Liquid C5+ hydrocarbon and CH4 selectivity variations with time on stream for the Co/GNS and Co/CNT catalysts (T = 220oC, P = 1.8MPa, H2/CO = 2)

References

1. Adesina AA. Hydrocarbon synthesis via Fischer-Tropsch reaction: travails and triumphs. Applied Catalysis A: General. 1996;138(2):345-67.
2. Dry ME. The Fischer–Tropsch process: 1950–2000. Catalysis today. 2002;71(3):227-41.
3. Li T, Wang H, Yang Y, Xiang H, Li Y. Study on an iron–nickel bimetallic Fischer–Tropsch synthesis catalyst. Fuel Processing Technology. 2014;118:117-24.

4. Medina C, García R, Reyes P, Fierro J, Escalona N. Fischer Tropsch synthesis from a simulated biosyngas feed over Co (x)/SiO 2 catalysts: Effect of Co-loading. Applied Catalysis A: General. 2010;373(1):71-5.
5. Feyzi M, Irandoust M, Mirzaei AA. Effects of promoters and calcination conditions on the catalytic performance of iron–manganese catalysts for Fischer–Tropsch synthesis. Fuel Processing Technology. 2011;92(5):1136-43.
6. Panpranot J, Kaewkun S, Praserthdam P, Goodwin Jr JG. Effect of cobalt precursors on the dispersion of cobalt on MCM-41. Catalysis letters. 2003;91(1-2):95-102.
7. Li J, Cheng X, Zhang C, Yang Y, Li Y. Effects of alkali on iron-based catalysts for Fischer-Tropsch synthesis: CO chemisorptions study. Journal of Molecular Catalysis A: Chemical. 2015;396:174-80.
8. Rytter E, Holmen A. Deactivation and Regeneration of Commercial Type Fischer-Tropsch Co-Catalysts—A Mini-Review. Catalysts. 2015;5(2):478-99
9. Asami K, Iwasa A, Igarashi N, Takemiya S, Yamamoto K, Fujimoto K. Fischer–Tropsch synthesis over precipitated iron catalysts supported on carbon. Catalysis today. 2013;215:80-5.
10. Machado BF, Serp P. Graphene-based materials for catalysis. Catalysis Science & Technology. 2012;2(1):54-75.
11. Tavasoli A. Catalyst composition and its distribution effects on the enhancement of activity, selectivity and suppression of deactivation rate of FTS cobalt catalysts: Ph. D. Thesis, University of Tehran: Tehran, Iran; 2005.
12. Jacobs G, Patterson PM, Das TK, Luo M, Davis BH. Fischer–Tropsch synthesis: effect of water on Co/Al 2 O 3 catalysts and XAFS characterization of reoxidation phenomena. Applied Catalysis A: General. 2004;270(1):65-76.
13. Tavasoli A, Mortazavi Y, Khodadadi A, Sadagiani K. Effects of different loadings of Ru and Re on physico-chemical properties and performance of 15% Co/Al2O3 FTS catalysts. Iranian Journal of Chemistry and. 2005.
14. Tavasoli A, Trépanier M, Dalai AK, Abatzoglou N. Effects of confinement in carbon nanotubes on the activity, selectivity, and lifetime of Fischer− Tropsch Co/carbon nanotube catalysts. Journal of Chemical & Engineering Data. 2010;55(8):2757-63.
15. Naeimi H, Mohajeri A, Moradi L, Rashidi AM. Efficient and facile one pot carboxylation of multiwalled carbon nanotubes by using oxidation with ozone under mild conditions. Applied Surface Science. 2009;256(3):631-5.
16. Serp P, Corrias M, Kalck P. Carbon nanotubes and nanofibers in catalysis. Applied Catalysis A: General. 2003;253(2):337-58.
17. Chen W, Fan Z, Pan X, Bao X. Effect of confinement in carbon nanotubes on the activity of Fischer− Tropsch iron catalyst. Journal of the American Chemical Society. 2008;130(29):9414-9.
18. Trépanier M, Dalai AK, Abatzoglou N. Synthesis of CNT-supported cobalt nanoparticle catalysts using a microemulsion technique: role of nanoparticle size on reducibility, activity and selectivity in Fischer–Tropsch reactions. Applied Catalysis A: General. 2010;374(1):79-86.
19. Tavasoli A, Karimi S, Taghavi S, Zolfaghari Z, Amirfirouzkouhi H. Comparing the deactivation behaviour of Co/CNT and Co/γ-Al 2 O 3 nano catalysts in Fischer-Tropsch synthesis. Journal of Natural Gas Chemistry. 2012;21(5):605-13.
20. Tavasoli A, Sadagiani K, Khorashe F, Seifkordi A, Rohani A, Nakhaeipour A. Cobalt supported on carbon nanotubes—a promising novel Fischer–Tropsch synthesis catalyst. Fuel Processing Technology. 2008;89(5):491-8.
21. Tavasoli A, Irani M, Nakhaeipour A, Mortazavi Y, Khodadadi AA, Dalai AK. Preparation of a Novel Super Active Fischer-Tropsch Cobalt Catalyst Supported on Carbon Nanotubes. Iran J Chem Chem Eng Vol. 2009;28(1).
22. Tavasoli A, Abbaslou RMM, Dalai AK. Deactivation behavior of ruthenium promoted Co/γ-Al 2 O 3 catalysts in Fischer–Tropsch synthesis. Applied Catalysis A: General. 2008;346(1):58-64.
23. Trépanier M, Tavasoli A, Dalai AK, Abatzoglou N. Co, Ru and K loadings effects on the activity and selectivity of carbon nanotubes supported cobalt catalyst in Fischer–Tropsch synthesis. Applied Catalysis A: General. 2009;353(2):193-202.
24. Tavasoli A, Abbaslou RMM, Trepanier M, Dalai AK. Fischer–Tropsch synthesis over cobalt catalyst supported on carbon nanotubes in a slurry reactor. Applied Catalysis A: General. 2008;345(2):134-42.
25. Chen G, Li S, Su Y, Wang V, Mizuseki H, Kawazoe Y. Improved stability and catalytic properties of Au16 cluster supported on graphane. The Journal of Physical Chemistry C. 2011;115(41):20168-74.
26. Davari M, Karimi S, Tavasoli A, Karimi A. Enhancement of activity, selectivity and stability of CNTs-supported cobalt catalyst in Fischer–Tropsch via CNTs functionalization. Applied Catalysis A: General. 2014;485:133-42.
27. Trépanier M, Tavasoli A, Anahid S. Deactivation Behavior of Carbon Nanotubes Supported Cobalt Catalysts in Fischer-Tropsch Synthesis. Iran J Chem Chem Eng Vol. 2011;30(1).
28. Chen W, Fan Z, Pan X, Bao X. Effect of confinement in carbon nanotubes on the activity of Fischer− Tropsch iron catalyst. Journal of the American Chemical Society. 2008;130(29):9414-9.
29. Pan X, Fan Z, Chen W, Ding Y, Luo H, Bao X. Enhanced ethanol production inside carbon-nanotube reactors containing catalytic particles. Nature materials. 2007;6(7):507-11.
30. Pan X, Bao X. Reactions over catalysts confined in carbon nanotubes. Chemical communications. 2008(47):6271-81.
31. Pendyala VRR, Graham UM, Jacobs G, Hamdeh HH, Davis BH. Fischer–Tropsch Synthesis: Morphology, Phase Transformation, and Carbon-Layer Growth of Iron-Based Catalysts. ChemCatChem. 2014;6(7):1952-60.
32. Shi B, Davis BH. Fischer–Tropsch synthesis: the paraffin to olefin ratio as a function of carbon number. Catalysis today. 2005;106(1):129-31.
33. Liu F, Sun J, Zhu L, Meng X, Qi C, Xiao F-S. Sulfated graphene as an efficient solid catalyst for acid-catalyzed liquid reactions. Journal of Materials Chemistry. 2012;22(12):5495-502.
34. Tavasoli A, Irani M, Abbaslou RMM, Trépanier M, Dalai AK. Morphology and deactivation behaviour of Co–Ru/γ-Al2O3 Fischer–Tropsch synthesis catalyst. The Canadian Journal of Chemical Engineering. 2008;86(6):1070-80.
35. Tavasoli A, Nakhaeipour A, Sadaghiani K. Raising Co/Al 2 O 3 catalyst lifetime in Fischer–Tropsch synthesis by using a novel dual-bed reactor. Fuel processing technology. 2007; 88(5):461-9.
36. Ma W, Jacobs G, Ji Y, Bhatelia T, Bukur DB, Khalid S, et al. Fischer–Tropsch synthesis: influence of CO conversion on selectivities, H2/CO usage ratios, and catalyst stability for a Ru promoted Co/Al2O3 catalyst using a slurry phase reactor. Topics in Catalysis. 2011; 54(13-15):757-67.
37. Bezemer GL, Bitter JH, Kuipers HP, Oosterbeek H, Holewijn JE, Xu X, et al. Cobalt particle size effects in the Fischer-Tropsch reaction studied with carbon nanofiber supported catalysts. Journal of the American Chemical Society. 2006; 128(12):3956-64.
38. Zhao H, Zhu Q, Gao Y, Zhai P, Ma D. Iron oxide nanoparticles supported on pyrolytic graphene oxide as model catalysts for Fischer Tropsch synthesis. Applied Catalysis A: General. 2013; 456:233-9.
39. Leenaerts O, Partoens B, Peeters F. Water on graphene: Hydrophobicity and dipole moment using density functional theory. Physical Review B. 2009; 79(23):235440.
40. Bartholomew CH. Mechanisms of catalyst deactivation. Applied Catalysis A: General. 2001; 212(1):17-60.